Control of a Single-Phase Cascaded H-Bridge Multilevel Inverter for Grid-Connected Photovoltaic Systems

Elena Villanueva, Pablo Correa, *Member, IEEE*, José Rodríguez, *Senior Member, IEEE*, and Mario Pacas, *Senior Member, IEEE*

***Abstract*—This paper presents a single-phase cascaded H-bridge converter for a grid-connected photovoltaic (PV) application. The multilevel topology consists of several H-bridge cells connected in series, each one connected to a string of PV modules. The adopted control scheme permits the independent control of each dc-link voltage, enabling, in this way, the tracking of the maximum power point for each string of PV panels. Additionally, low-ripple sinusoidal-current waveforms are generated with almost unity power factor. The topology offers other advantages such as the operation at lower switching frequency or lower current ripple compared to standard two-level topologies. Simulation and experimental results are presented for different operating conditions.**

***Index Terms*—Multilevel inverters, photovoltaic (PV) power systems, power conversion.**

I. Introduction

GRID-CONNECTED single-phase photovoltaic (PV) systems are nowadays recognized for their contribution to clean power generation. A primary goal of these systems is to increase the energy injected to the grid by keeping track of the maximum power point (MPP) of the panel, by reducing the switching frequency, and by providing high reliability. In addition, the cost of the power converter is also becoming a decisive factor, as the price of the PV panels is being decreased [1]. This has given rise to a big diversity of innovative converter configurations for interfacing the PV modules with the grid. Currently, the state-of-the-art technology is the two-level multistring converter. This converter consists of several PV strings that are connected with dc–dc converters to a common dc–ac converter [2], [3]. This topology features several advantages such as the independent tracking of the MPP of each string and the possibility to scale the system by plugging more strings to the existing plant. This converter topology can reach peak efficiencies up to 96% [4].

In the last years, multilevel converter topologies have been also considered in PV applications [5]. These converter topologies can generate high-quality voltage waveforms with power semiconductor switches operating at a frequency near the fundamental [6]. Although, in low-power applications, the switching frequency of the power switches is not restricted, a low switching frequency can increase the efficiency of the converter [7]. Additionally, multilevel converters feature several dc links, making possible the independent voltage control and the tracking of the MPP in each string. This characteristic can increase the efficiency of the PV system in case of mismatch in the strings, due to unequal solar radiation, aging of the PV panels, and different type of the cells or accumulation of dust in the surface of the panels [8].

Among the available multilevel converter topologies, the cascaded multilevel converter constitutes a promising alternative, providing a modular design that can be extended to allow a transformerless connection to the grid [9], [10]. Additionally, this topology features power semiconductors with a lower rating than the standard two-level configurations, allowing cost savings [5]. Last but not the least, multilevel topologies feature several freedom degrees that make possible the operation of the converter even under faulty conditions, increasing, in this way, the reliability of this system [11]. In spite of all these characteristics, the cascaded multilevel topology has also disadvantages, as the strings of PV panels are not grounded and extra measures have to be taken in order to avoid currents due to stray capacitances between the panel and the earth [9].

In order to properly operate a cascaded converter with n cells, the independent control of the dc-link voltages and the control of the grid current i_S (Fig. 1) are necessary. This task must be accomplished by using the n available actuation signals corresponding to the modulation units of each cell. Several methods have been proposed to the control of this configuration. In [12]–[14], the reference signals for the modulation units of each cell are multiplied by a factor that depends on the voltage in each dc link and the power that the corresponding string of PV panels is delivering. Unfortunately, no experimental results are given. Other approaches operate only under equal dc-link voltages [15], which is not adequate for the tracking of the MPP in each string. In [16] and [17], control methods based on passivity controllers have been presented. The experimental

Manuscript received November 29, 2008; revised July 28, 2009. First published August 28, 2009; current version published October 9, 2009. This work was supported in part by the Universidad Técnica Federico Santa María and in part by the Chilean Research Council under Grant FONDECYT 1080582.

E. Villanueva, P. Correa, and J. Rodríguez are with the Electronics Engineering Department, Universidad Técnica Federico Santa María, Valparaíso 2390123, Chile (e-mail: elena.villanueva@usm.cl; pablo.correa@usm.cl; jrp@usm.cl).

M. Pacas is with the Institute of Power Electronics and Electrical Drives, Faculty of Electrical Engineering and Computer Sciences, University of Siegen, 57068 Siegen, Germany (e-mail: jmpacas@ieee.org).

Color versions of one or more of the figures in this paper are available online at http://ieeexplore.ieee.org.

Digital Object Identifier 10.1109/TIE.2009.2029579

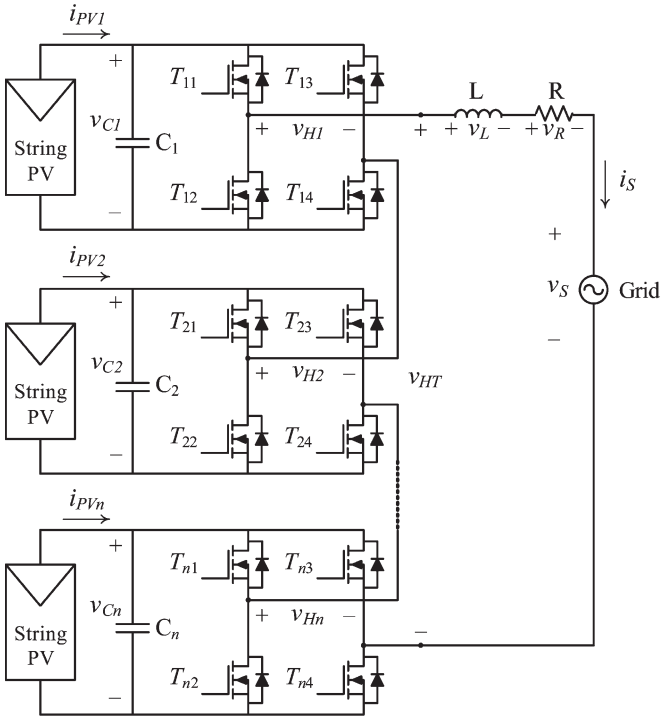

Fig. 1. Topology for grid connection.

results show that independent control of the dc-link voltages is possible. However, the equations for the controller are not explicitly described, and high-performance control platforms are required for real-time implementation of the proposed control schemes.

In this paper, a simple scheme based on the algorithm presented in [18] is applied for the control of a PV cascaded converter system. The control scheme is enhanced with MPP-tracking (MPPT) algorithms that independently adjust the reference of the dc-link voltages in order to maximize the generated energy. In addition, the quality of the grid currents is improved by using, for the measurement of the dc voltages, a digital 100-Hz band reject filter.

This paper is organized as follows. First, the converter topology is presented in Section II. Then, the control principle is explained in Section III. The model necessary for the design of the controllers is described in Section IV. The last section shows the simulation and experimental results that validate the proper operation of the converter. The results demonstrate that this topology can inject to the grid sinusoidal input currents with unity power factor, even under conditions of unequal solar radiation of the string of PV cells.

II. Topology Description

The cascaded multilevel converter topology consists of n H-bridge converters connected in series, as shown in Fig. 1. Each dc link is fed by a short string of PV panels. By considering cells with the same dc-link voltage, the converter can synthesize an output voltage $v_{\rm HT}$ with n levels. This high-quality voltage waveform enables the reduction of the harmonics in the generated current, reducing the filtering effort at the input.

The output voltage is easily determined from the following relation:

$$v_{Hj} = (T_{j1} - T_{j3}) \cdot v_{Cj} = P_j \cdot v_{Cj}, \qquad j = 1, \ldots, n \quad (1)$$

where $T_{\rm XX}$ represents the state of each switch according to Fig. 1. $T_{\rm XX}$ presents two discrete values: "1" when the switch is turned on and "0" when the switch is turned off. Therefore, P_j can have the discrete values -1, 0, or $+1$, when the output voltage of the H-bridge is $-v_c$, 0, or $+v_c$, respectively. In order to have a complete lineal model of the converter, the functions P_j are replaced by the continuous switching functions $S_j \in [-1, 1]$. Thus, the dynamic behavior of the system can be described by [18]

$$\frac{di_S}{dt} = \frac{1}{L}\left(\sum_{j=1}^{n}(S_j v_{Cj}) - Ri_S - v_S\right) \quad (2)$$

$$\frac{dv_{Cj}}{dt} = \frac{1}{C_j}(i_{{\rm PV}j} - S_j i_S), \qquad j = 1, \ldots, n. \quad (3)$$

III. Control Scheme

The control strategy is based in the classical scheme for the control of a single H-bridge converter connected to the grid. In [12]–[18], this idea has been extended for the case of n cells connected in series for the control of an active rectifier. From these different control schemes, only [16]–[18] seems to be suited for this application because they are able to operate with different dc-link voltages. In this paper, the control scheme proposed in [18] is used for this application by adding MPPT controllers in the voltage reference.

The scheme in Fig. 2 includes $n + 1$ control loops: n of them are used to adjust the capacitor voltage in each dc link, and the other one is necessary for the generation of a sinusoidal input current with unity power factor. As shown in Fig. 2, the sum of the dc-link voltages v_{C1} to v_{Cn} is controlled through a PI that determines the amplitude of the input current $\hat{i}_S$. By multiplying the output of this controller with a normalized sinusoidal signal in phase with the voltage grid, a suitable reference for the current loop is obtained.

On the other hand, the PI current controller PI_i gives the sum of the continuous switching functions $S_1 + S_2 + \cdots + S_n$. The control of the voltages v_{C2} to v_{Cn} is made through another $n - 1$ controller that selects the switching function amplitude $\hat{S}_j$ directly. Note that this scheme sets the phase of S_2 to S_n equal to grid phase. This can be better understood for the case of two cells, as it is shown in Fig. 3. The power factor can be controlled either by changing the magnitude and phase of the voltage of the first cell or the magnitude of the voltage of the second cell. From now on, only the two-cell case will be considered for simplicity and to easily appreciate the working principle.

It is important to remark that the power factor control is limited by the number of cells and the value of the input inductance. Unity power factor is obtained when a voltage v_L with a phase of 90° with respect to the grid voltage is generated. Regardless of the number of cells, in this control scheme, only v_{H1} can produce the complex part of the phasor v_L. Hence, a

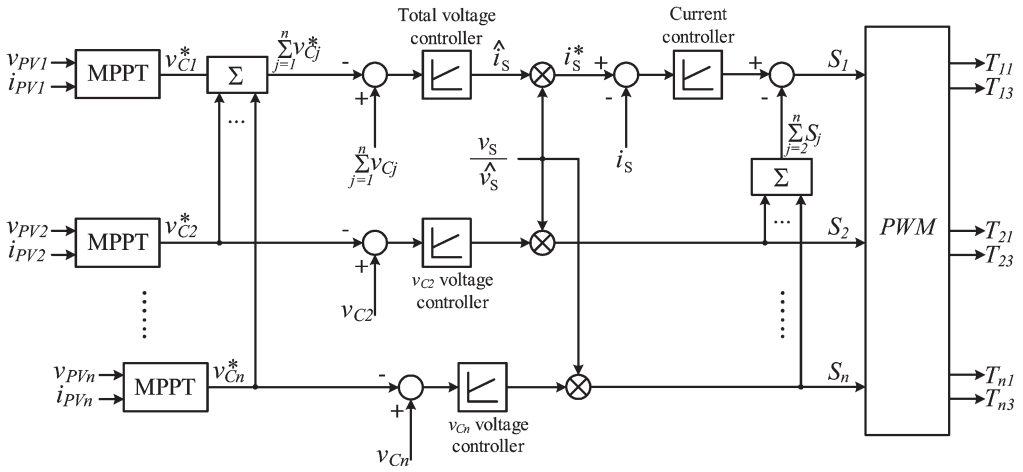

Fig. 2. Proposed control scheme.

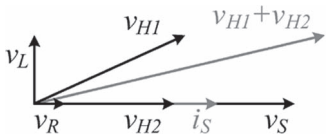

Fig. 3. Phasor diagram.

very high value of the filter inductance could make the problem of unity power factor unfeasible. To avoid this problem, $v_{H1} > v_L$ is required.

In order to obtain the maximum power from each PV panel, the Perturb and Observe (P&O) algorithm is used [19]. This algorithm is the most commonly used in practice because of its simple implementation and has the potential to be very competitive with other methods if it is properly optimized for the given hardware. The variables to observe are the calculated output power of the PV panels, and the variables to perturb are, in this case, the reference voltages, namely, v_{C1} and v_{C2}.

IV. System Modeling and Controller Design

In this section, the tuning procedure for the three control loops in Fig. 4 is described. The design of the filter for the mitigation of the 100-Hz harmonic component in the input current i_S is also addressed.

A. Current Loop

Since the dynamic of the current loop is much faster than the dynamic of the voltage loop, the design for the controller will mainly consider this dynamic and the delay time of the converter and the modulator. The plant is given by

$$G_i(s) = \frac{I_S(s)}{V_{\mathrm{HT}}(s)} = \frac{I_S(s)}{V_{H1}(s) + V_{H2}(s)} = \frac{1}{Ls + R}. \quad (4)$$

The simplified control scheme of the current control loop is shown in Fig. 4(a). The design of the current controller assumes that grid voltage v_S is a slowly variant disturbance for the current loop. For this reason, it will not be considered.

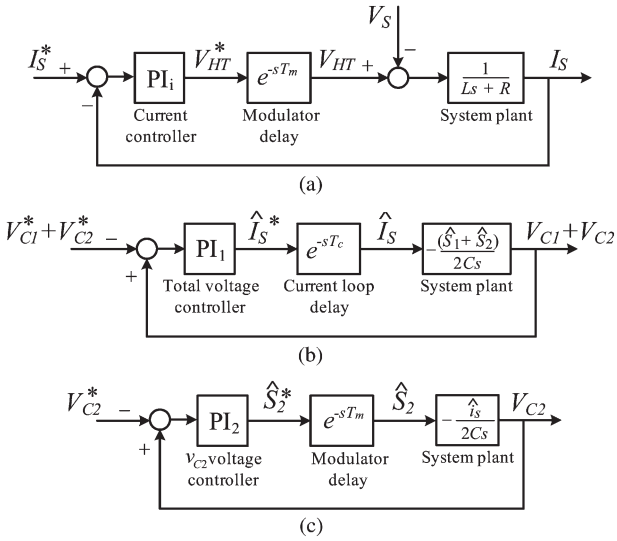

Fig. 4. (a) Current loop. (b) Total voltage loop. (c) Second cell voltage loop.

B. Voltage Loop

Two PI controllers are necessary for the independent control of each dc-link voltage. In order to design the controllers, suitable transfer functions are obtained by the linearization of (3) with $j = 1, 2$ around the nominal operating point. In this case, it will be considered that the system operates at a nominal radiation of 1 kW/m^2 and at 25 °C. As a first step, the transfer function of the loop that considers the total dc-link voltage will be calculated. The derivation of this expression is documented in [18] and reproduced here for the sake of completeness. Adding these two equations yields

$$S_1 i_S + S_2 i_S = i_{\mathrm{PV1}} + i_{\mathrm{PV2}} - C_1 \frac{dv_{C1}}{dt} - C_2 \frac{dv_{C2}}{dt}. \quad (5)$$

By considering only the dc component of the term $S_1 \cdot i_S + S_2 \cdot i_S$, the last equation is equivalent to

$$\frac{\hat{S}_1 \hat{i}_S + \hat{S}_2 \hat{i}_S}{2} = i_{\mathrm{PV1}} + i_{\mathrm{PV2}} - C_1 \frac{dv_{C1}}{dt} - C_2 \frac{dv_{C2}}{dt} \quad (6)$$

where $\hat{x}$ indicates the maximum value of x.

In order to simplify the transfer function, the currents of the PV panels i_{PV1} and i_{PV2} will be considered as disturbances and the term $\hat{S}_1 + \hat{S}_2$ constant. Under this assumptions, the following transfer function is obtained:

$$\frac{V_{C1}(s) + V_{C2}(s)}{\hat{I}_S(s)} = -\frac{(\hat{S}_1 + \hat{S}_2)}{2Cs} \tag{7}$$

where $C_1 = C_2 = C$ and the term $\hat{S}_1 + \hat{S}_2$ is defined for nominal operating conditions, as it is indicated in the Appendix.

The second voltage control loop is necessary to adjust the voltage difference between both dc-link voltages. Equation (3), with $j = 2$ with same considerations of the previous loop, provides the basis for the design of the controller. In this case, it will be assumed that the current magnitude delivered by the first control loop is constant; thus

$$\frac{V_{C2}(s)}{\hat{S}_2(s)} = -\frac{\hat{I}_S}{2Cs} \tag{8}$$

where $\hat{I}_S$ is defined for nominal steady state conditions, as it is shown in the Appendix. The schemes for the two voltage loops are shown in Fig. 4(b) and (c).

The design of the three PI controllers has been carried out with root locus method in the Laplace domain [20]. The current controller was designed using a bandwidth of 400 rad/s, which is high enough to provide an adequate current tracking and filter the harmonics of the modulation. The voltage controllers were designed considering the frequency of the MPPT algorithm, which, in this case, is equal to 10 Hz. For these controllers, a bandwidth between 63 and 200 rad/s was considered.

C. Mitigation of the 100-Hz Harmonic Component in the Input Currents

Using this control configuration, a harmonic component of the triple of the fundamental frequency appears in the input current i_S. In order to mitigate this harmonic component in the current, a band reject filter centered in 100 Hz has been placed between the voltage measurements v_{C1} and v_{C2} and the inputs of voltage controllers, as shown in Fig. 6. In this way, the 150-Hz harmonic component is eliminated from the current references. Note that filters between PV voltage measurements and MPPT blocks are intentionally avoided because it is necessary to assure the proper tracking of the optimum power point.

The digital filters work according to the principle shown in Fig. 5. The original signal $V(t)$ is delayed a half cycle and then added to the original waveform to obtain the dc component of the signal [21]. A block diagram of the complete control scheme, including the two 100-Hz filters, is shown in Fig. 6.

V. Results

In order to validate the proposed ideas, simulation and experimental tests were carried out. In both cases, a setup consisting

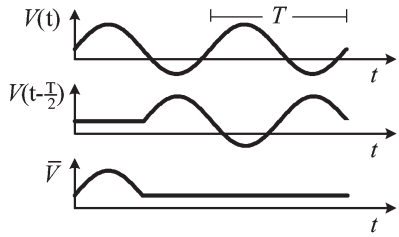

Fig. 5. Filter principle.

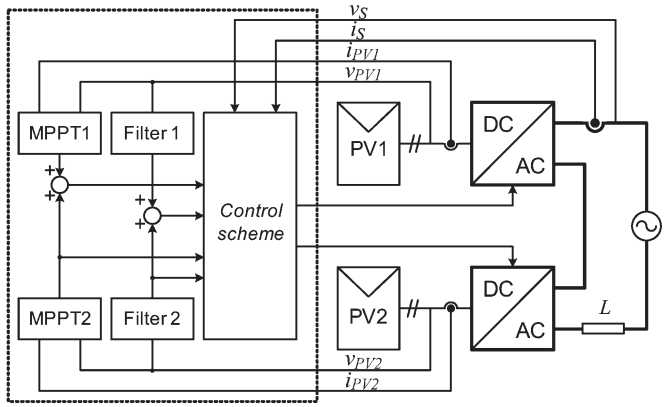

Fig. 6. Proposed control scheme with MPPT and band reject filters.

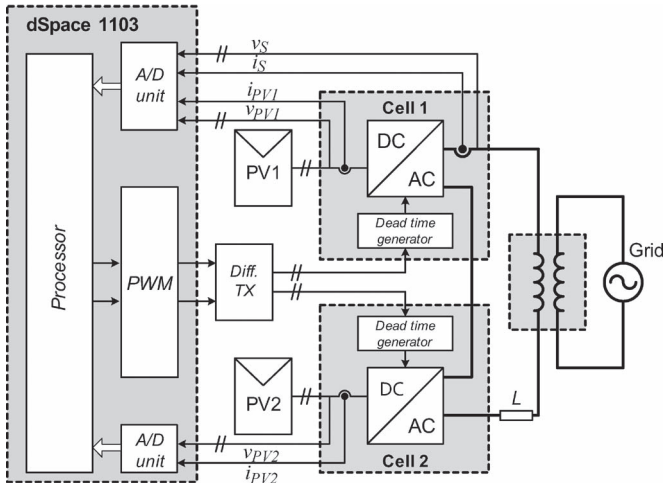

Fig. 7. Experimental setup.

in two H-bridge inverters connected in series was considered, as shown in Fig. 1. Each H-bridge inverter includes only one PV panel so the voltage that can be generated by the system is lower than the grid voltage. For this reason, a transformer was added between the inverter and the grid in order to reach the grid voltage levels, as it is shown in Fig. 7.

In order to allow a transformerless grid connection, the maximum dc voltage of the converter must be higher than the grid voltage value for any condition. For example, by considering a two-cell converter, a grid voltage of 220 V and PV panels that can deliver 23 V in the worst radiation conditions, a string of at least seven panels connected to each cell is needed to fulfill this requirement.

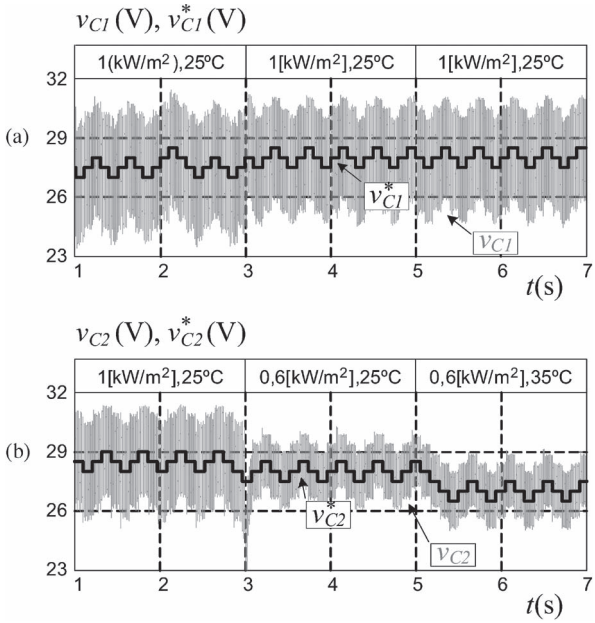

Fig. 8. DC-link voltages. (a) Cell 1. (b) Cell 2.

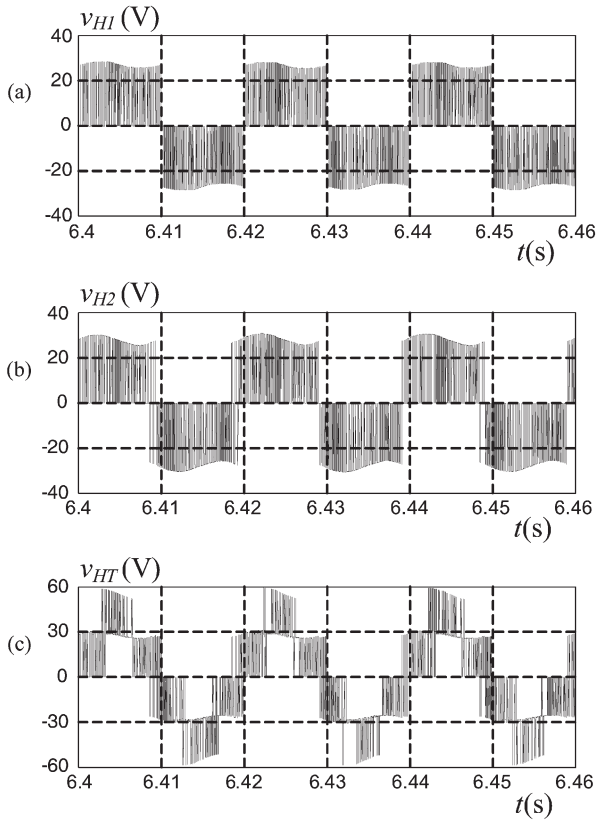

Fig. 9. Output voltages. (a) Cell 1. (b) Cell 2. (c) Whole inverter.

A. Simulation Results

The PV panel was modeled according to the specification of the commercial PV panel from Sharp, type 208U2. The dc-link capacitor considered in this paper is of 4700 μF for each module, and the ac filter has the parameters $L = 1$ mH and $R = 0.1\ \Omega$. The input transformer provides a 30-V peak at the terminals.

The modulation of each cell is done using unipolar pulsewidth modulation (PWM) generated by using a triangular carrier signal with a frequency $f_{\rm cr} = 5$ kHz. The multilevel waveform is generated using phase-shifted PWM (PS-PWM) [22].

The simulation is carried out in Matlab–Simulink, where the converter is modeled according to (1)–(3). The control parameters used in the simulation are listed in the Appendix. The operation of the five-level inverter is simulated for three different operating conditions, as shown in Fig. 8. In the first one, both temperature and solar radiation are equal for the two PV panels with 25 °C and 1 kW/m^2. At $t = 3$ s, the solar radiation over the second panel decreases to 0.6 kW/m^2. Finally, at $t = 5$ s, the temperature in the second panel increases from 25 °C to 35 °C. In the three different operating conditions, the MPPT gives references around the optimum point in only three levels according to the P&O algorithm best results [19]. The dc-link voltages follow the references after a short transient. Whereas the MPP voltage of the first cell does not change because the operating point in the whole simulation is the same, a lower radiation in the second PV affects the current that the string delivers to the cell, as it can be observed in the lower ripple of the dc-link between $t = 3$ s and $t = 5$ s in Fig. 8(b). The change in the temperature affects also the mean value of the MPP voltage [23], as it can be observed between $t = 5$ s and $t = 7$ s in the same figure.

Fig. 9(a) and (b) shows the characteristic three-level voltage output of each cell. These voltages in series connection form the five-level voltage at the output of the inverter shown in Fig. 9(c). The number of levels depends of the dc-link voltage of each cell. A higher number of levels can be expected if the strings are operating in different conditions. In addition, if v_{C1} is not equal to v_{C2}, low-frequency harmonics around $2f_c$ appear in the whole inverter voltage $v_{\rm HT}$ spectrum. The distortion added by these harmonics to the current i_s is not significant because the energy remains concentrated in the high-frequency harmonics.

Fig. 10(a) shows the voltage and current at the terminals of the transformer. The current is in phase with the voltage but clearly has the harmonic component of 150 Hz. Fig. 10(b) shows the same variables, but in this case, the harmonic reject filter is used in the dc-link voltage measurements, resulting in a current without noticeable harmonic components.

B. Experimental Results

The simulation results were also validated with an experimental setup with the same configuration. The control was implemented in fast prototype platform dSpace 1103. This controller features a floating point processor, 20 analog/digital converter inputs, and two PWM units. Fig. 11(a) shows a photo of the H-bridge cell, and Fig. 11(b) shows the PV panel Sharp 208U2 that was used for the experimental validation.

In order to evaluate the behavior of the control method under different radiation conditions, one panel was covered by a mesh. Fig. 12(a)–(d) shows the reference voltage of each dc

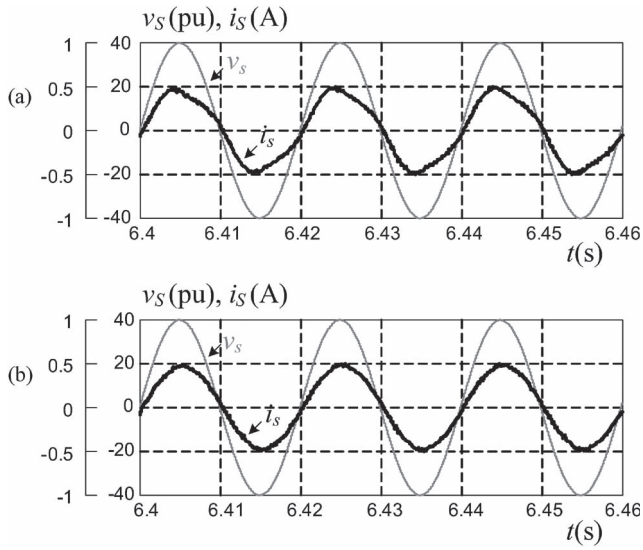

Fig. 10. Voltage and current in the terminals of the transformer. (a) Without filter. (b) With 100-Hz band filter.

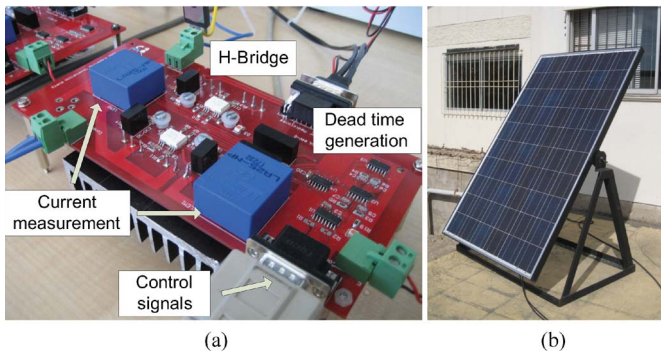

Fig. 11. (a) H-bridge cell. (b) Sharp 208U2 PV panel.

link and the measured and filtered voltages. In both cases, the MPPT algorithm gives a reference with three levels around the V_{MPP} voltage (the MPP voltage for specific PV panel) which is followed after a small transient.

The different operating points of the cells are reflected in the amount of dc-link voltage ripple, as shown in Fig. 12(a) and (c). The first PV panel generates higher currents than the second one; for this reason, the voltage variation is higher as predicted by (2) and (3).

The current delivered to the transformer is shown in Fig. 12(e) together with the normalized voltage used for synchronization. The current presents a displacement factor of 0.95 and a THDc $= 5.5\%$. Although the THD index is higher than the 5% permitted by the norm, part of this distortion is caused by the current reference, which is obtained from the voltage. The grid voltage has, in this case, high amounts of fifth and seventh harmonic components that produce a THDv of 4.3%. Better results can be expected with a less distorted grid or by using a phase-locked loop to generate the current reference. On the other hand, the displacement factor of 0.95 is explained by the use of a high-value filter inductance in the laboratory prototype, according to the comments in Section III.

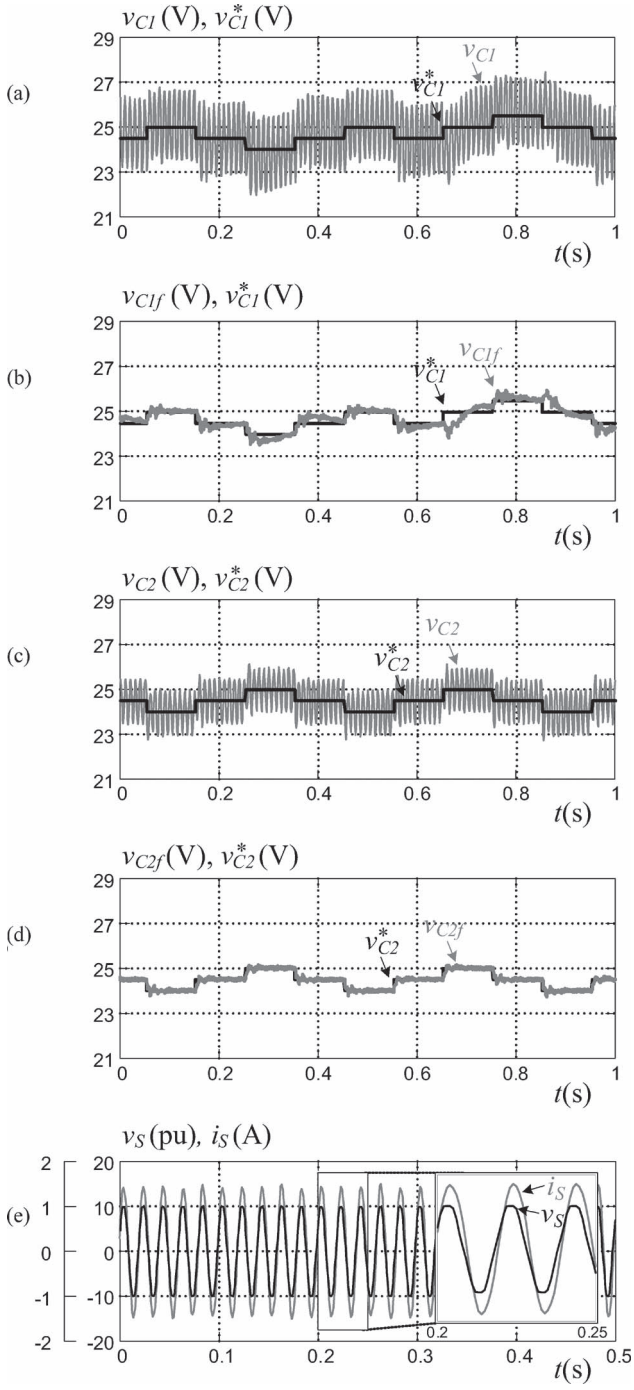

Fig. 12. DC-link voltages. (a) Reference and measurement in cell 1. (b) Reference and measurement with the 100-Hz reject band filter in cell 1. (c) Reference and measurement in cell 2. (d) Reference and measurement with the 100-Hz reject band filter in cell 2. (e) Voltage and grid current.

VI. Conclusion

In this paper, a cascaded H-bridge multilevel converter has been proposed as a feasible multistring topology for PV applications. The converter features several advantages such as the generation of high-quality currents, the capacity to operate at a lower switching frequency than a two-level converter, and the modularity that can reduce the cost of the solution. The converter is first controlled using a scheme proposed for multilevel active rectifiers and improved by adding MPPT algorithms.

TABLE I
CONTROLLER PARAMETERS

Control loop	Simulation		Experimental	
	P	I	P	I
Grid current	0.288	0.012	0.07	0.004
Total voltage	0.99	0.01	0.25	0.002
v_{C2} voltage	0.0297	0.0003	0.2	0.002

Whereas the original method was proposed for constant dc-link voltages, this application makes full use of the capacity of the control scheme to independently adjust the dc-link voltages. This permits the individual tracking of the MPP of each PV string of panels. The control scheme was enhanced by adding a filter to eliminate the 150-Hz component in the currents.

Experimental and simulation results, with a setup consisting in two cells and two PV panels, indicate that the converter can operate properly even in conditions with different radiation of the strings and generate sinusoidal currents with almost unity power factor.

APPENDIX

For the calculation of $\hat{i}_S$, the power balance between the input and the output of the converter is used. The following expression defines $P_{\rm in}$ and $P_{\rm out}$, where the losses in the capacitor and MOSFETs have been neglected:

$$P_{\rm in} = i_{\rm PV1} v_{C1} + i_{\rm PV2} v_{C2} - \frac{1}{2} R \hat{i}_S^2 \tag{9}$$

$$P_{\rm out} = \frac{1}{2} \hat{v}_S \hat{i}_S. \tag{10}$$

Considering that both PV modules are working in the same operation point, (9) and (10) are equal

$$P_{\rm in} = P_{\rm out}$$

$$2 i_{\rm PV} v_C - \frac{1}{2} R \hat{i}_S^2 = \frac{1}{2} \hat{i}_S \hat{v}_S. \tag{11}$$

Finally, the following expression for $\hat{i}_S$ is obtained:

$$\hat{i}_S = -\frac{\hat{v}_S}{2R} + \sqrt{\frac{\hat{v}_S^2}{4R^2} + \frac{4 i_{\rm PV} v_C}{R}}. \tag{12}$$

The value of $\hat{S}_1 + \hat{S}_2$ is derived from the phasor relation described in Fig. 3. Considering only the amplitude of the phasors, the following expression can be obtained:

$$(\hat{v}_{H1} + \hat{v}_{H2})^2 = (\hat{v}_S + \hat{i}_S R)^2 + (\omega L \hat{i}_S)^2. \tag{13}$$

Considering that $v_{C1} = v_{C2} = v_C$, (13) can be written as

$$(\hat{S}_1 + \hat{S}_2)^2 v_C^2 = (\hat{v}_S + \hat{i}_S R)^2 + (\omega L \hat{i}_S)^2. \tag{14}$$

Then, $\hat{S}_1 + \hat{S}_2$ becomes

$$\hat{S}_1 + \hat{S}_2 = \sqrt{\frac{(\hat{v}_S + \hat{i}_S R)^2}{v_C^2} + (\omega L \hat{i}_S)^2 v_C^2}. \tag{15}$$

When $\hat{i}_S$ and $\hat{S}_1 + \hat{S}_2$ are calculated, the operation point is the MPP of each panel; therefore, MPP values for current and voltage at 1 kW/m^2 are used, i.e., $i_{\rm PV} = i_{\rm MPP}$ and $v_C = v_{\rm MPP}$.

The discrete PI control parameters used in simulation and experimental results are described in Table I.

REFERENCES

[1] S. Kjaer, J. Pedersen, and F. Blaabjerg, "A review of single-phase grid-connected inverters for photovoltaic modules," *IEEE Trans. Ind. Appl.*, vol. 41, no. 5, pp. 1292–1306, Sep./Oct. 2005.

[2] M. Meinhardt and G. Cramer, "Multi-string converter: The next step in evolution of string-converter technology," in *Proc. 9th Eur. Conf. Power Electron. Appl.*, 2001. [CD-ROM].

[3] S. Khajehoddin, A. Bakhshai, and P. Jain, "A novel topology and control strategy for maximum power point trackers and multi-string grid-connected PV inverters," in *Proc. 23rd Annu. IEEE APEC*, Feb. 2008, pp. 173–178.

[4] Sunny Boy 5000tl Multi-String Operating Instructions, SMA, Niestetal, Germany, Oct. 2008. [Online]. Available: www.sma.de

[5] S. Daher, J. Schmid, and F. Antunes, "Multilevel inverter topologies for stand-alone PV systems," *IEEE Trans. Ind. Electron.*, vol. 55, no. 7, pp. 2703–2712, Jul. 2008.

[6] J. Rodriguez, J.-S. Lai, and F. Z. Peng, "Multilevel inverters: A survey of topologies, controls, and applications," *IEEE Trans. Ind. Electron.*, vol. 49, no. 4, pp. 724–738, Aug. 2002.

[7] E. Ozdemir, S. Ozdemir, L. Tolbert, and B. Ozpineci, "Fundamental frequency modulated multilevel inverter for three-phase stand-alone photovoltaic application," in *Proc. 23rd Annu. IEEE APEC*, Feb. 2008, pp. 148–153.

[8] S. Busquets-Monge, J. Rocabert, P. Rodriguez, S. Alepuz, and J. Bordonau, "Multilevel diode-clamped converter for photovoltaic generators with independent voltage control of each solar array," *IEEE Trans. Ind. Electron.*, vol. 55, no. 7, pp. 2713–2723, Jul. 2008.

[9] M. Calais and V. Agelidis, "Multilevel converters for single-phase grid connected photovoltaic systems—An overview," in *Proc. IEEE ISIE*, Jul. 1998, vol. 1, pp. 224–229.

[10] H. Ertl, J. Kolar, and F. Zach, "A novel multicell DC–AC converter for applications in renewable energy systems," *IEEE Trans. Ind. Electron.*, vol. 49, no. 5, pp. 1048–1057, Oct. 2002.

[11] P. Correa, M. Pacas, and J. Rodriguez, "Predictive torque control for inverter-fed induction machines," *IEEE Trans. Ind. Electron.*, vol. 54, no. 2, pp. 1073–1079, Apr. 2007.

[12] O. Alonso, P. Sanchis, E. Gubia, and L. Marroyo, "Cascaded H-bridge multilevel converter for grid connected photovoltaic generators with independent maximum power point tracking of each solar array," in *Proc. 34th Annu. IEEE PESC*, Jun. 2003, vol. 2, pp. 731–735.

[13] J. Negroni, F. Guinjoan, C. Meza, D. Biel, and P. Sanchis, "Energy-sampled data modeling of a cascade H-bridge multilevel converter for grid-connected PV systems," in *Proc. 10th IEEE Int. Power Electron. Congr.*, Oct. 2006, pp. 1–6.

[14] S. Khajehoddin, A. Bakhshai, and P. Jain, "The application of the cascaded multilevel converters in grid connected photovoltaic systems," in *Proc. IEEE EPC*, Montreal, QC, Canada, Oct. 2007, pp. 296–301.

[15] B.-R. Lin and H.-H. Lu, "New multilevel rectifier based on series connection of H-bridge cell," *Proc. Inst. Elect. Eng.—Electr. Power Appl.*, vol. 147, no. 4, pp. 304–312, Jul. 2000.

[16] C. Cecati, A. Dell'Aquila, M. Liserre, and V. Monopoli, "A passivity-based multilevel active rectifier with adaptive compensation for traction applications," *IEEE Trans. Ind. Appl.*, vol. 39, no. 5, pp. 1404–1413, Sep./Oct. 2003.

[17] D. Noriega-Pineda and G. Espinosa-Perez, "Passivity-based control of multilevel cascade inverters: High performance with reduced switching frequency," in *Proc. IEEE ISIE*, Jun. 2007, pp. 3403–3408.

[18] A. Dell'Aquila, M. Liserre, V. Monopoli, and P. Rotondo, "Overview of pi-based solutions for the control of DC buses of a single-phase H-bridge multilevel active rectifier," *IEEE Trans. Ind. Appl.*, vol. 44, no. 3, pp. 857–866, May/Jun. 2008.

[19] D. P. Hohm and M. E. Ropp, "Comparative study of maximum power point tracking algorithms," *Prog. Photovolt.: Res. Appl.*, vol. 11, no. 1, pp. 47–62, Jan. 2003.

[20] G. C. Goodwin, S. F. Graebe, and M. E. Salgado, *Control System Design*. Englewood Cliffs, NJ: Prentice-Hall, 2000.

[21] A. Saleh, M. Pacas, and A. Shaltout, "Fault tolerant field oriented control of the induction motor for loss of one inverter phase," in *Proc. 32nd IEEE IECON*, Nov. 2006, pp. 817–822.
[22] J. Rodriguez, S. Bernet, B. Wu, J. Pontt, and S. Kouro, "Multilevel voltage-source-converter topologies for industrial medium-voltage drives," *IEEE Trans. Ind. Electron.*, vol. 54, no. 6, pp. 2930–2945, Dec. 2007.
[23] J. Gow and C. Manning, "Development of a photovoltaic array model for use in power-electronics simulation studies," *Proc. Inst. Elect. Eng.—Electr. Power Appl.*, vol. 146, no. 2, pp. 193–200, Mar. 1999.

Elena Villanueva received the Engineer and M.Sc. degrees in electronic engineering from the Universidad Técnica Federico Santa María (UTFSM), Valparaíso, Chile, in 2008.

She is currently with the Electronics Engineering Department, UTFSM. Her research interests include power electronics and renewable energy systems.

Pablo Correa (M'07) received the Engineer degree in electrical engineering from the Universidad Técnica Federico Santa María (UTFSM), Valparaíso, Chile, in 2001, and the Dr. Ing. degree from the University of Siegen, Siegen, Germany, in 2006, with a scholarship awarded in 2002 by the German Academic Exchange Service for doctoral studies.

Currently he is a Postdoctoral Research Fellow in the Electronics Engineering Department of the UTFSM. His research interests include digital control for high-power drives and renewable energy converters and the development of high-performance control platforms based on field-programmable gate arrays.

José Rodríguez (M'81–SM'94) received the Engineer degree in electrical engineering from the Universidad Técnica Federico Santa María, Valparaíso, Chile, in 1977, and the Dr. Ing. degree in electrical engineering from the University of Erlangen, Erlangen, Germany, in 1985.

Since 1977, he has been with the Electronics Engineering Department, University Técnica Federico Santa María, where he is currently a Professor and was the Director from 2001 to 2004. From 2004 to 2005, he was the Vice Rector of academic affairs, and since 2005, he has been the Rector. During his sabbatical leave in 1996, he was responsible for the Mining Division, Siemens Corporation, Santiago, Chile. He has extensive consulting experience in the mining industry, particularly in the application of large drives such as cycloconverter-fed synchronous motors for semiautogenous grinding mills, high-power conveyors, and controlled ac drives for shovels and power-quality issues. He has directed more than 40 R&D projects in the field of industrial electronics. He has coauthored more than 250 journal and conference proceedings papers and contributed one book chapter. His research group was recognized as one of the two Centers of Excellence in Engineering in Chile from 2005 to 2008. His main research interests include multilevel inverters, new converter topologies, and adjustable-speed drives.

Prof. Rodríguez has been an active Associate Editor of the IEEE TRANSACTIONS ON POWER ELECTRONICS and IEEE TRANSACTIONS ON INDUSTRIAL ELECTRONICS since 2002. He has served as Guest Editor for the IEEE TRANSACTIONS ON INDUSTRIAL ELECTRONICS in five instances [Special Sections on Matrix Converters (2002), Multilevel Inverters (2002), Modern Rectifiers (2005), High Power Drives (2007), and Predictive Control of Power Converters and Drives (2008)].

Mario Pacas (SM'00) received the Dipl.Ing. and Dr. Ing. degrees in electrical engineering from the University of Karlsruhe, Karlsruhe, Germany, in 1978 and 1985, respectively.

From 1985 to 1995, he was with Brown Boveri & Cie/Asea Brown Bovri (ABB) in Switzerland and Germany in different R&D and management positions with very wide experience in international projects. In his last years with ABB, he was responsible for the development of servodrives and was later the Product Responsible Manager for these products. Since 1996, he has been a member of the Faculty of Electrical Engineering and Computer Sciences, University of Siegen, Siegen, Germany, where he heads the Institute of Power Electronics and Electrical Drives. His special fields of interest are motion control, diagnostics, system identification, and optimization of mechatronic systems.